



**Supplementary Information for**

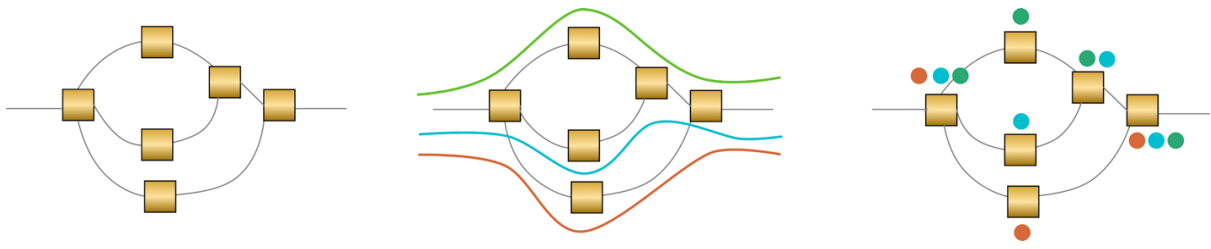
Novel functional sequences uncovered through a bovine multi-assembly graph

Danang Crysanto\*, Alexander S. Leonard, Zih-Hua Fang, Hubert Pausch  
Animal Genomics, ETH Zürich, Zürich, Switzerland

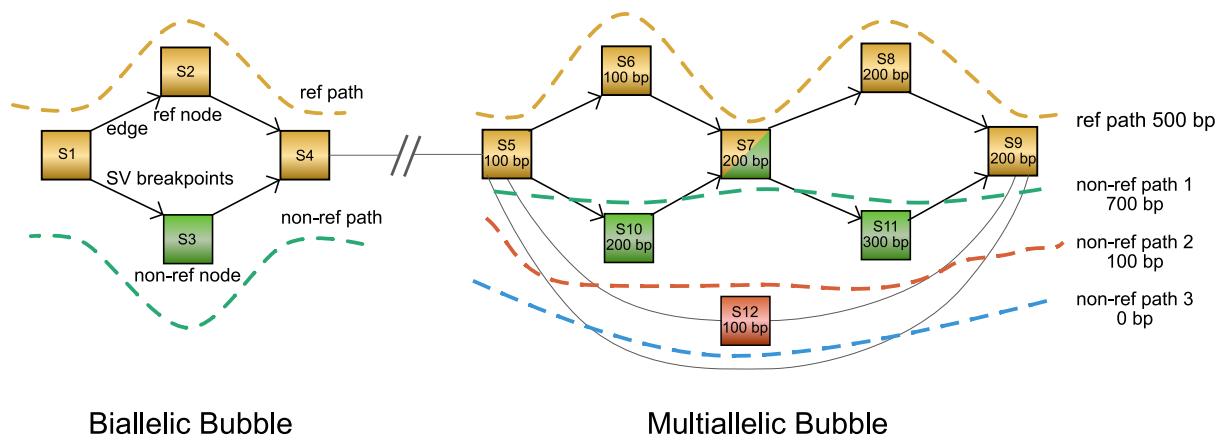
\*Corresponding author: Danang Crysanto, danang.crysanto@usys.ethz.ch

**This PDF file includes:**

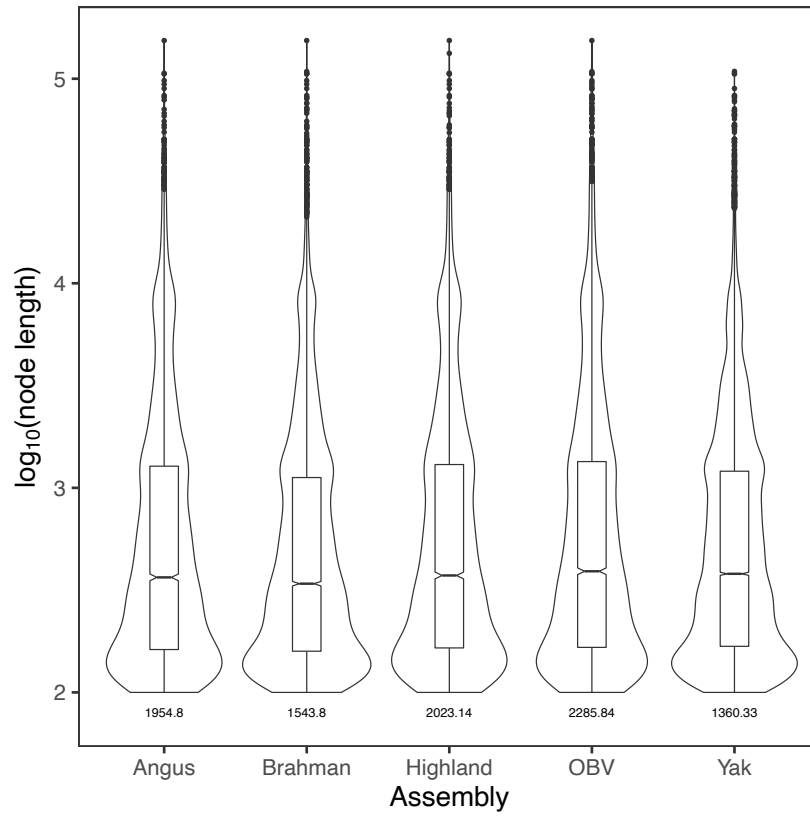
**Supplementary Figure S1-S14**  
**Supplementary Table S1-S5**  
**Supplementary Note S1-S5**  
**SI References**



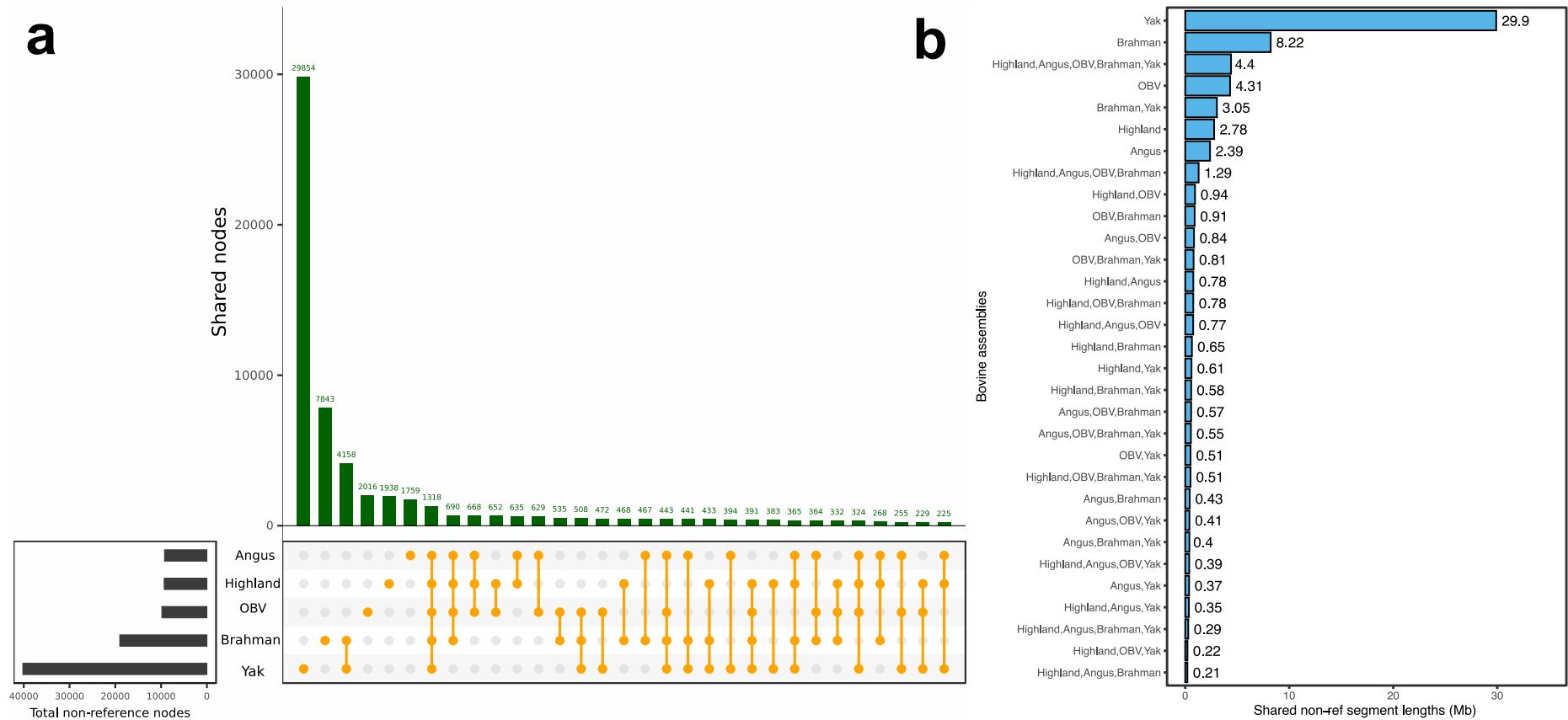
**Supplementary Figure 1. Labelling of the nodes in the multi-assembly graph.** To determine the support for the nodes in the graph, we aligned each individual assembly back to the multi-assembly graph and labeled nodes according to the assembly paths that traversed them with different colors. The left panel represents a schematic graph. Rectangles and lines represent nodes and edges, respectively. The middle panel represents the paths of three assemblies traversing the nodes. The right panel displays how each node that was traversed by an assembly receives a label (colored dots).



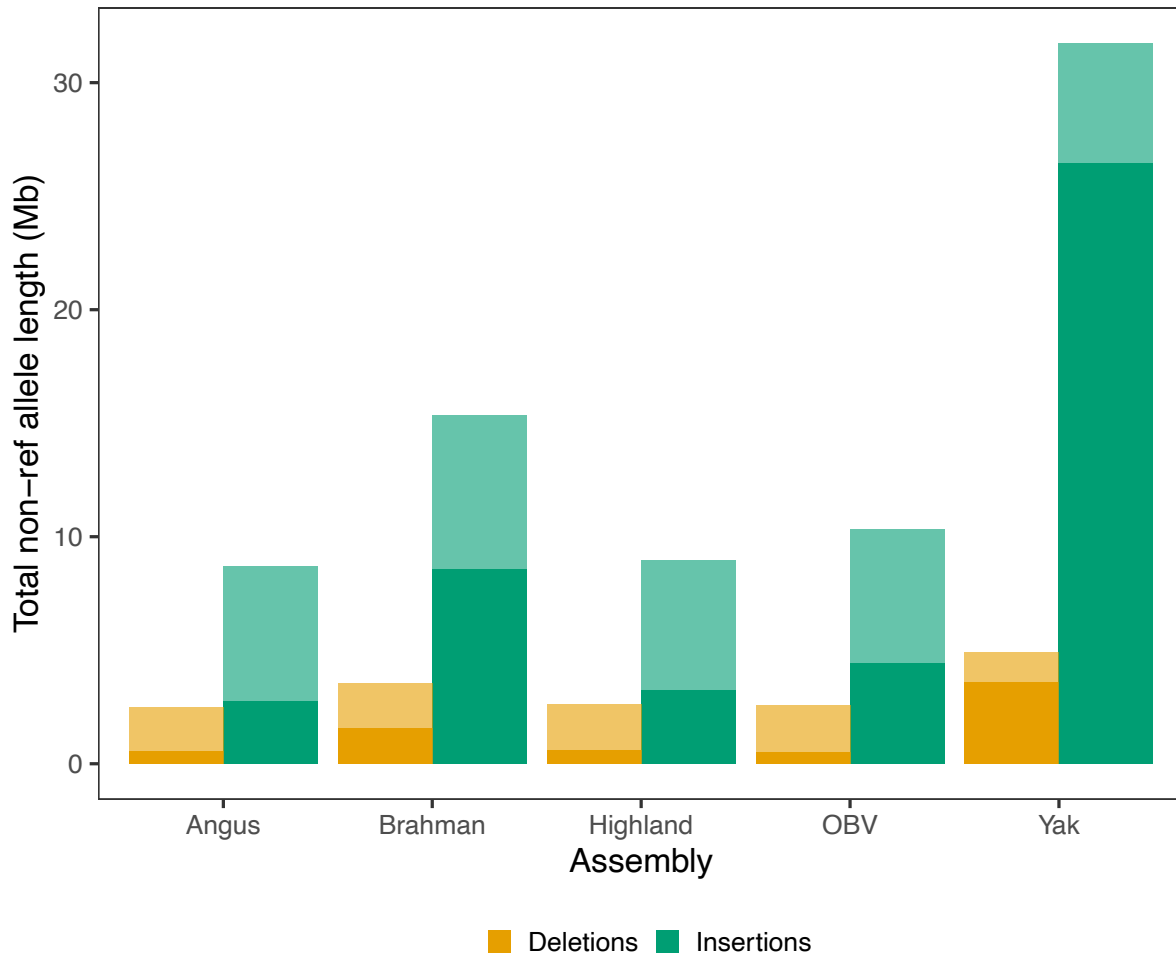
**Supplementary Figure 2. Graphs and structural variants terminology used in the paper.** (*left*) A node contains a sequence of nucleotides (S1-S12). Reference nodes (S1, S2, S4) are derived from the backbone assembly used to construct the graph. Non-reference nodes (S3) contain sequences from additional assemblies that are not present in the backbone. Nodes are connected by directed edges from parent to child where the underlying sequences are contiguous. Edges between reference and non-reference nodes are breakpoints of structural variations. Bubbles are branching regions in the graph which start and end at reference nodes. (*right*) Paths in the bubbles represent different alleles of structural variations, which are biallelic if a bubble contains two paths or multiallelic if it contains more. Nodes within biallelic bubbles represent alleles. Within multi-allelic bubbles, multiple nodes may be part of the same path and thus allele. It is worth noting that not all combinations of nodes within bubbles are real paths found in individual assemblies (e.g., S10-S7-S8). As such, color-consistent nodes within a bubble are stitched together to represent true paths. By comparing reference and non-reference paths, it is possible to determine the type of the structural variations (e.g., non-ref path 1: alternate insertion, path 2: alternate deletion, path 3: complete deletion).



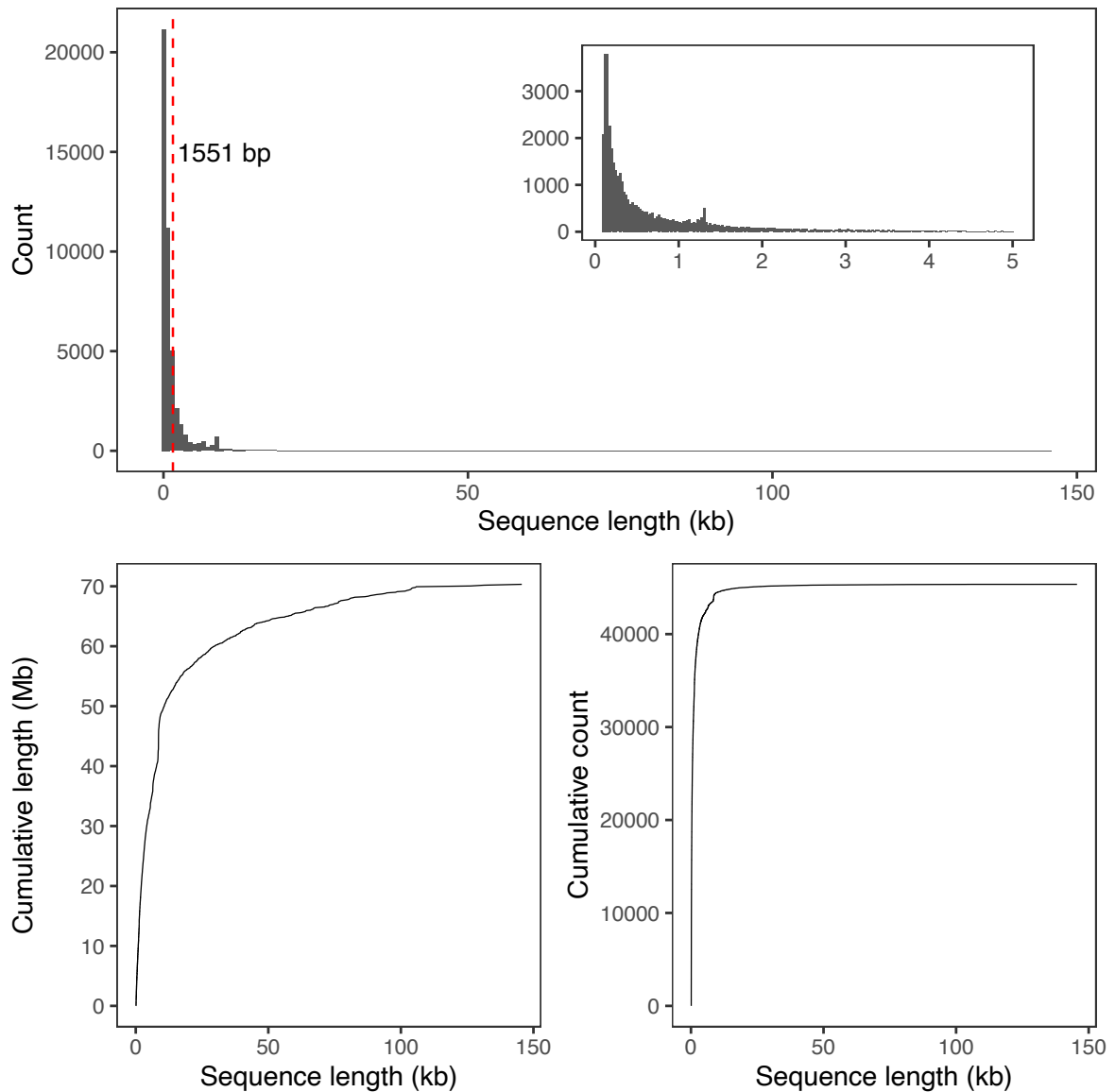
**Supplementary Figure 3. The size of non-reference nodes labelled with each of the five assemblies.** The Y-axis is  $\log_{10}$ -scaled. Numbers below each plot refer to the average non-reference node length from each assembly.



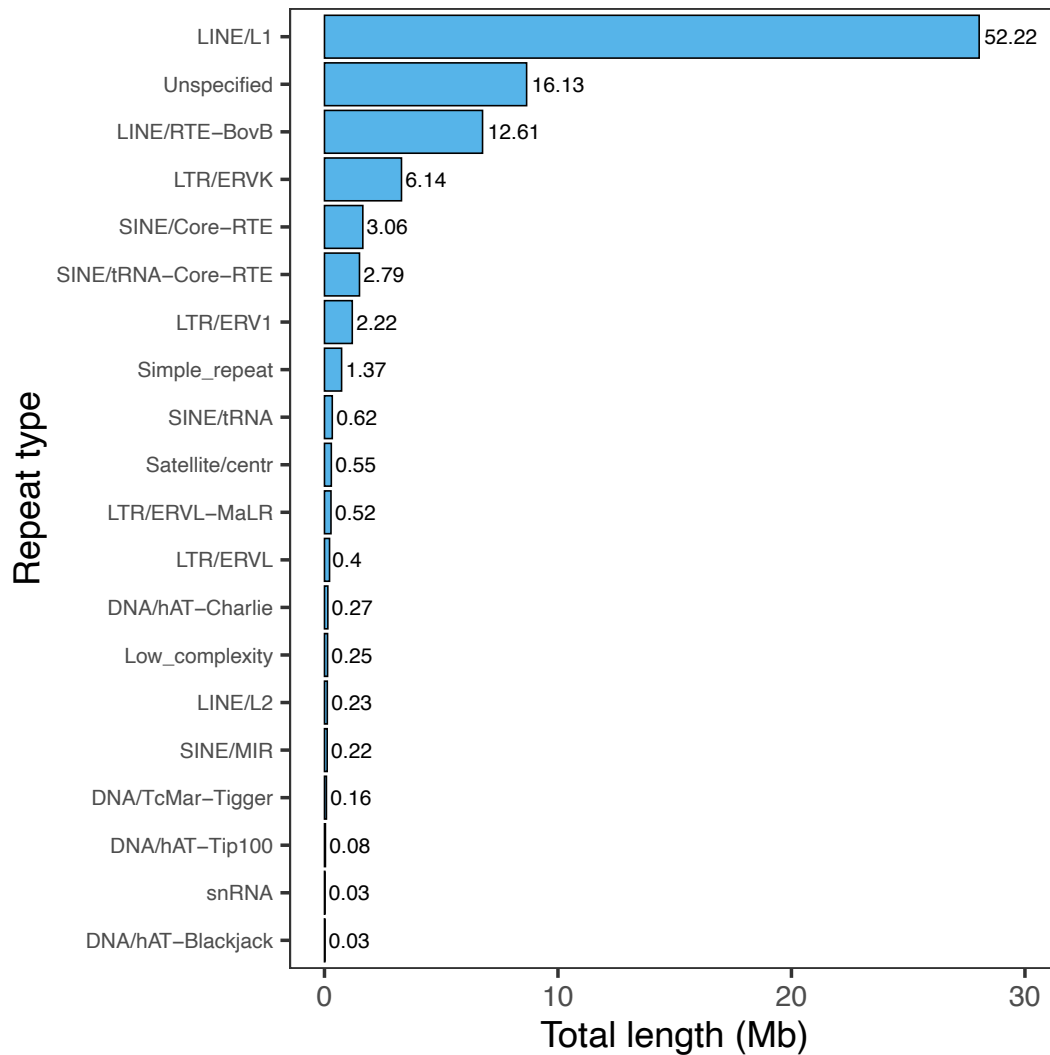
**Supplementary Figure 4. Non-reference nodes detected across assemblies.** Intersection of non-reference nodes (a) and cumulative length of non-reference sequences (b) found in five assemblies when compared to ARS-UCD1.2. OBV = Original Braunvieh.



**Supplementary Figure 5. Deletion and insertion polymorphism detected from each assembly in the pangenome graph.** Transparent and solid bars indicate the total and private length of non-reference alleles respectively. OBV – Original Braunvieh.

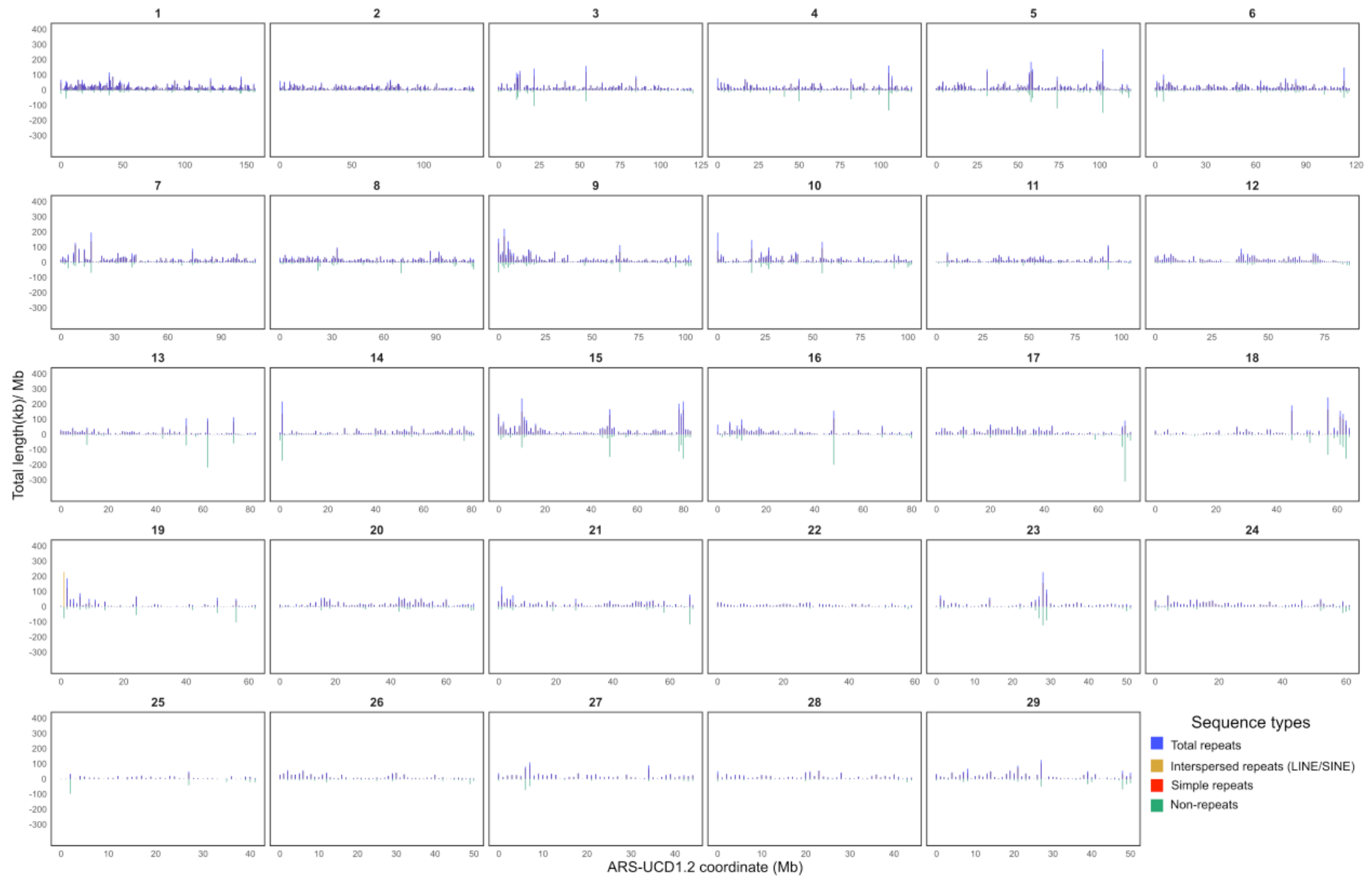


**Supplementary Figure 6. Length of the non-reference sequences that were added linearly to the ARS-UCD1.2 reference.** Length distribution of the non-reference alleles (upper panel) and their cumulative length and count (lower panels). The inset in the upper panel displays the distribution of non-reference alleles shorter than 5 kb. The dashed-red line indicates the average length (1551 bp) of the non-reference alleles.

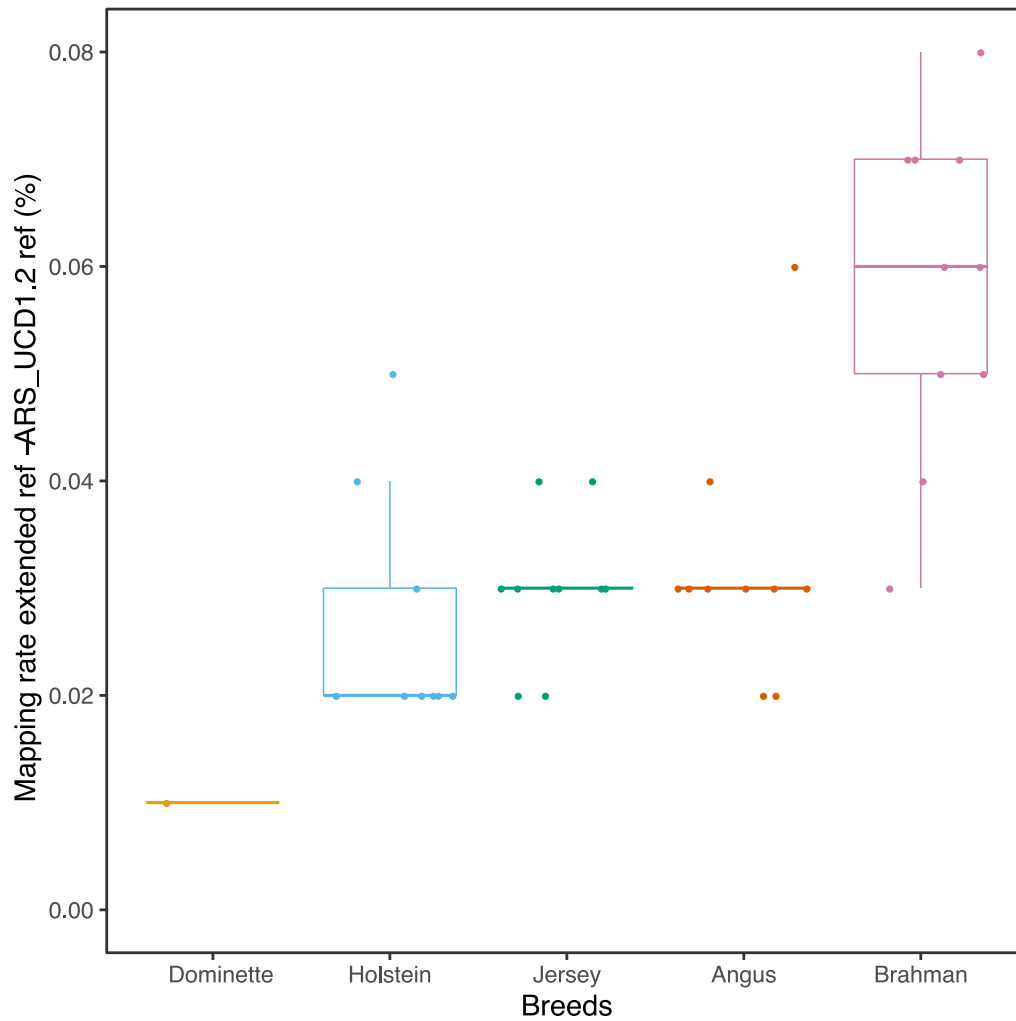


**Supplementary Figure 7. Prevalence of repetitive elements in the non-reference sequences.** The 20 most prevalent repetitive elements account for 99.9% of the repetitive elements detected in the non-reference sequences. The X-axis indicates the summed sequence length (in Mb) spanned by the repetitive elements, with text labels indicate the proportion (%) of a repetitive element contributing to the total repeat length.



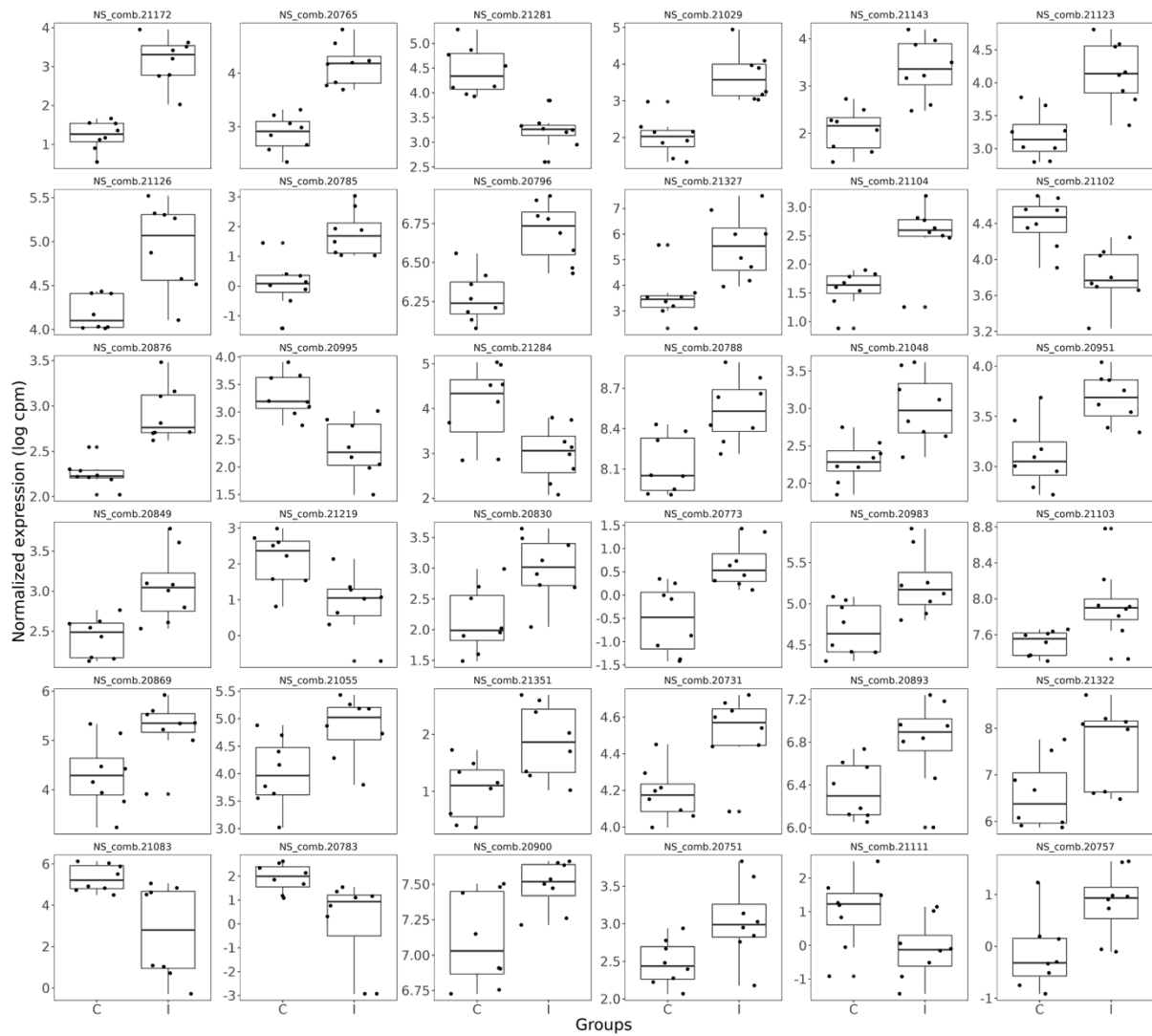


**Supplementary Figure 8.** The distribution of repetitive element (interspersed and simple repeats), and non-repetitive elements found in non-reference sequences based on the ARS-UCD1.2 coordinate system. To aid visualization, the distribution of non-repetitive segments is mirrored to the negative Y-axis. The numbers above the individual panels are chromosome identifiers.

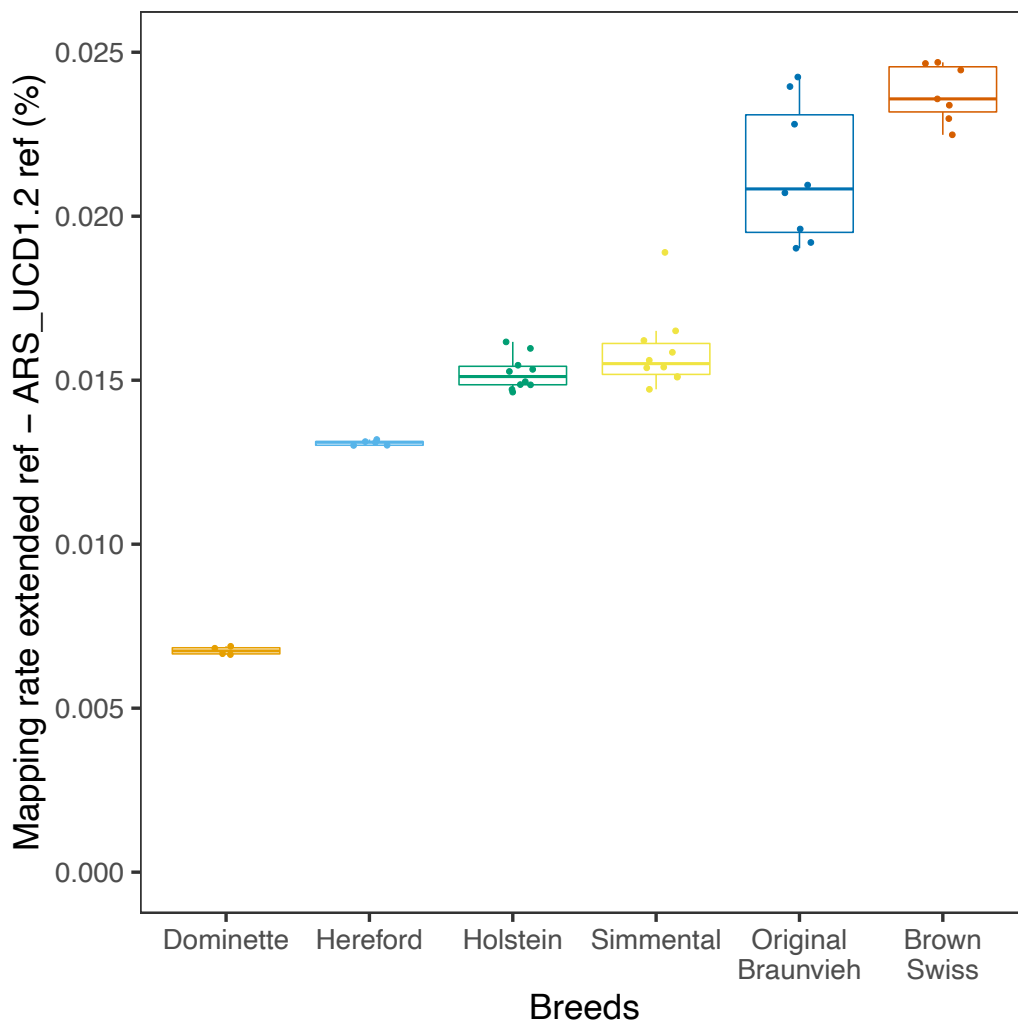


**Supplementary Figure 9. Transcriptome mapping rate improvements in five breeds using the extended reference sequence over ARS-UCD1.2.** Values along the Y axis represent the difference in mapping rate between the extended and the original ARS-UCD1.2 reference (%) as reported by HISAT2. Positive values indicate that more reads aligned to the extended than original reference. Dominette is the Hereford animal used to construct ARS-UCD1.2.

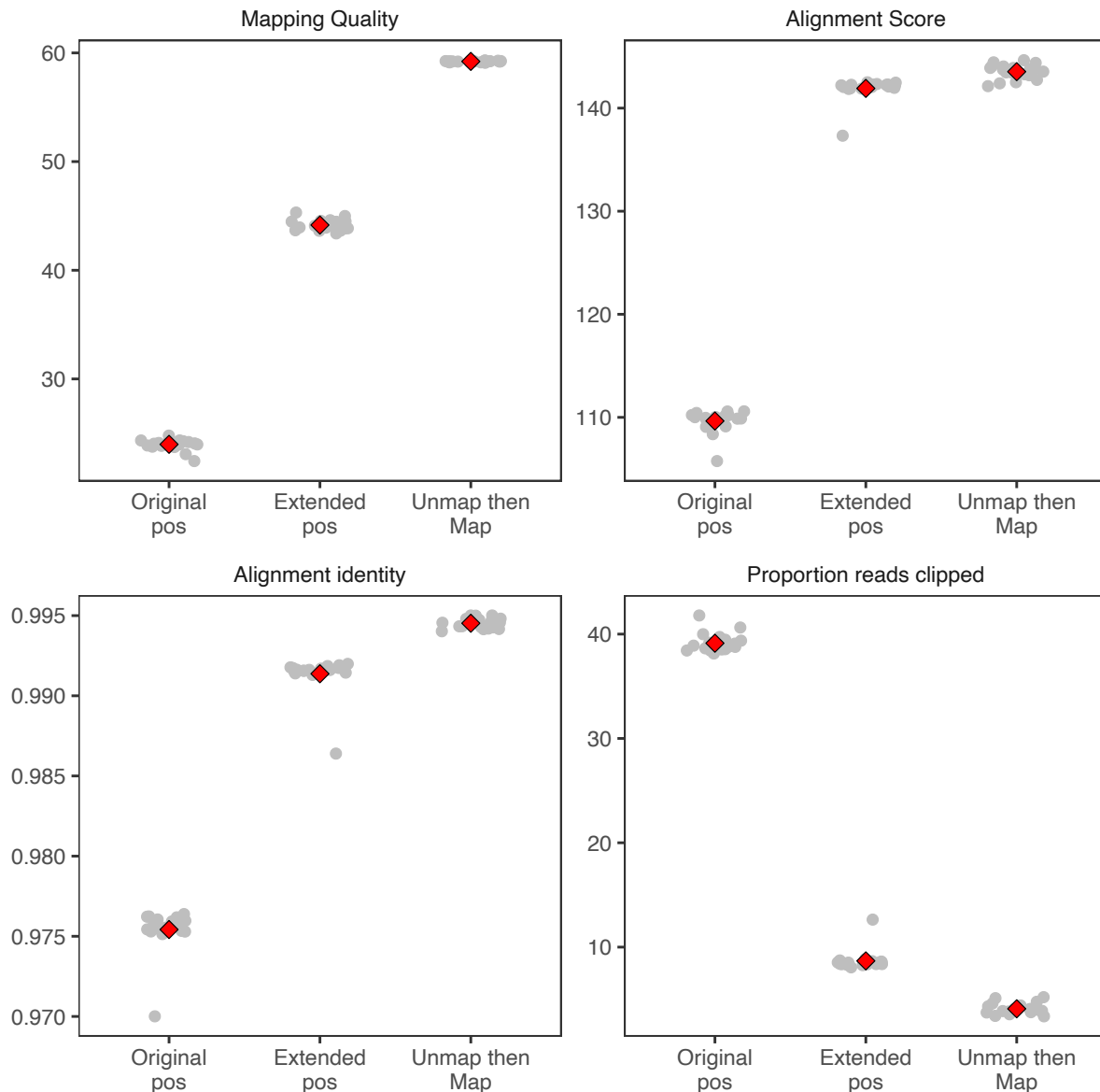




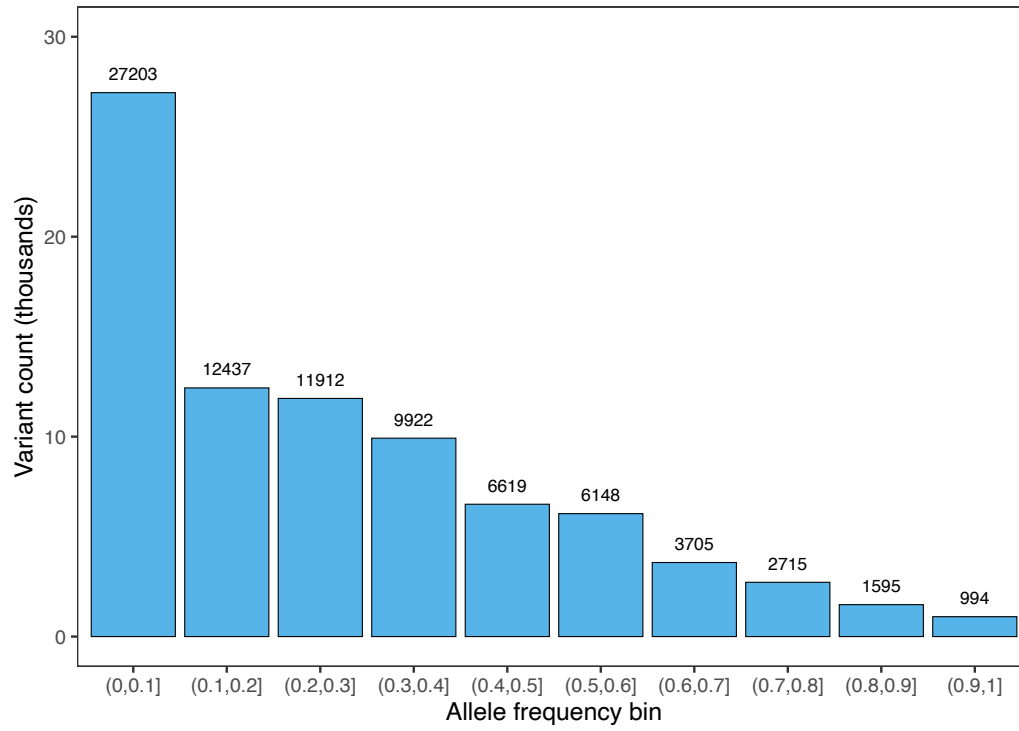
**Supplementary Figure 11. Differential expression of 36 non-reference genes in *Mycobacterium bovis*-infected cattle.** Control (C) and *Mycobacterium bovis*-infected (I) cattle are grouped separately for each gene. Y axis indicates the normalized transcript abundance expressed as log<sub>2</sub> CPM as reported by EdgeR.



**Supplementary Figure 12. Mapping rate of whole-genome short sequencing reads to the extended linear reference genome.** The Y-axis reflects the difference (in %) in mapping rate between the extended reference and the original ARS–UCD1.2 reference sequences. Positive values indicate that the mapping rate is higher for samples aligned to the extended than original ARS-UCD1.2 reference sequences. Short sequencing reads of 45 cattle from five breeds were considered. Dominette is a Hereford cattle, but is separated as she is the animal used to construct ARS-UCD1.2.



**Supplementary Figure 13. Accuracy of read mapping to non-reference sequences.** Four mapping statistics (mapping quality, alignment score, alignment identity, proportion of clipped reads) were assessed for short sequencing reads from 45 samples across 5 breeds. First, we consider reads that mapped to autosomal sequences of the ARS-UCD1.2. The mapping statistics of these reads are compared between the ARS-UCD1.2 reference sequence (Original pos) and their mapping position at the novel non-reference sequences of the extended reference genome (Extended pos). Second, we consider reads that were unmapped against the ARS-UCD1.2 reference genome but received a mapping position against the extended reference genome (Unmap then map). Each grey point indicates the average mapping statistics for one DNA sample and red diamond indicates the average across all animals.



**Supplementary Figure 14. Alternate allele frequency of 83,250 variants detected from non-reference sequences in 45 samples from 5 breeds.**

**Supplementary Table 1. Different types of structural variations discovered from the multi-assembly graph.** Variant length is calculated based on the absolute difference between reference and non-reference allele.

<b>Mutations</b>	<b>Types</b>	<b>Count</b>	<b>Complete type</b>	<b>Alternate type</b>	<b>Non-ref allele length</b>	<b>Variant length</b>
Insertions	biallelic	35748	20432	15316	40361474	37388222
Insertions	multiallelic	4621	4221	400	21116534	10303720
Deletions	biallelic	28476	15377	13099	2845080	28373582
Deletions	multiallelic	4661	1972	2689	10130841	11727721
<b>Total</b>		<b>73506</b>	<b>42002</b>	<b>31504</b>	<b>74453929</b>	<b>87793245</b>



**Supplementary Table 2. Gene model prediction from repeat masked non-reference sequences.** Total novel genes denote all gene models (including partial genes) predicted by Augustus. Complete gene models restricted to only full gene models (TSS, start codon, exon, intron, stop-codon present). Transcript, exon, and CDS statistics reported as mean (maximum-minimum) length from the full gene models.

<b>Feature of the gene model</b>	<b>Value</b>
Total novel genes (distinct SVs)	857 (768)
Complete novel genes (distinct SVs)	374 (328)
Transcript length (bp)	4742.14 (min: 314; max: 104024)
Exon length (bp)	942.30 (min: 15; max: 6725)
Exon length/gene (bp)	2050.89 (min: 314; max: 7762)
Exon count/gene (bp)	2.18 (min: 1; max: 20)
CDS length (bp)	396.64 (min: 5; max: 3059)
CDS length/gene (bp)	794.34 (min: 199; max: 6280)
protein length (aa)	264.78 (min: 66.33; max: 2093.33)

**Supplementary Table 3. BLASTX hits of the transcripts from differentially expressed non-reference genes.** Log2 FC is the difference in expression between *Mycobacterium bovis*-infected and non-infected control cattle (e.g., a positive value indicates that expression is higher in infected than control cattle), and Adj FDR is the adjusted false discovery rate determined using the Benjamini-Hochberg correction.

Hits	Mean (SD) expression in CPM		log2 FC	Adj FDR
	Control	Infected		
Antigen WC1.1-like	2.43 (0.6)	9.54 (3.65)	2.0137	1.98E-05
Leukocyte immunoglobulin-like receptor subfamily A member 5 isoform X1	23.10 (8.30)	9.59 (2.54)	-1.2870	0.0001
PREDICTED: synaptobrevin homolog YKT6	4.39 (1.36)	11.19 (4.7)	1.3754	0.0008
PREDICTED: major vault protein isoform X1	21.70 (3.87)	14.23 (2.88)	-0.6140	0.0040
PREDICTED: heat shock 70 kDa protein 1B	10.18 (2.7)	5.33 (1.94)	-0.9511	0.0041
Elongation factor 1-alpha 1	282.86 (40.74)	374.22 (63.08)	0.4033	0.0093
Heterogeneous nuclear ribonucleoprotein R isoform 2	5.47 (0.94)	8.65 (2.73)	0.6740	0.0148
PREDICTED: prothymosin alpha isoform X2	22.02 (10.73)	39.85 (12.84)	0.8523	0.0243
Stathmin isoform a	17.56 (7.39)	30.3 (10.17)	0.7823	0.0271
Serine/arginine repetitive matrix protein 1 isoform X1	18.3 (1.74)	22.99 (3.29)	0.3293	0.0285
BOLA class I histocompatibility antigen, alpha chain BL3-7-like	109.32 (61.3)	223.94 (116.59)	1.0387	0.0302
Predicted gene, EG665562	141.66 (31.9)	179.9 (20.92)	0.3440	0.0400
PREDICTED: GTP-binding protein SAR1a	5.71 (1.22)	8.71 (3.28)	0.6231	0.0415

**Supplementary Table 4. Comparison of read mapping accuracy between the extended and ARS-UCD1.2 reference.** All metrics were extracted from BAM files using pysam v0.16.0.1 (1). Alignment identity reflects the proportion of bases from an aligned read that match the reference sequence. A read was considered to be clipped if the CIGAR string of the alignment contains tags for either hard- (H) or soft-clipped (S) bases. Supplementary alignments were reported for alignments with an XS tag. Criteria for perfect and unique alignments were based on those reported by Crysanto and Pausch (2). Specifically, reads were considered to align perfectly if the edit distance was zero along the entire read (NM:0 tag), and when the CIGAR did not include H or S tags. Unique alignments are reported for reads that either have a single primary alignment or reads that have a secondary alignment (XA tag) but one alignment has a maximum mapping quality score of 60. Reported values are averaged over  $n=45$  samples. Paired one-sided t-tests were conducted with  $n-1$  degrees of freedom. Parameters marked with '\*' indicate the null-hypothesis that ARS-UCD1.2 would perform better than the extended reference, while those without marks indicate the reverse. All tests rejected the null hypothesis.

Parameter	Extended reference	ARS-UCD1.2	Difference	Stdev	t-statistic & p-value
Unmap (%) *	0.4291	0.4467	-0.0176	0.00461087	t = -24.12, p = 2.39e-25
Alignment identity 99% (%)	87.2716	87.1875	0.0841	0.00433417	t = 122.72, p = 2.19e-52
Alignment perfect (%)	68.5732	68.4687	0.1045	0.00667272	t = 99.04, p = 9.10e-49
Clipped alignment (%) *	2.1335	2.1923	-0.0588	0.00891613	t = -41.74, p = 2.81e-34
Supplementary alignment (%) *	0.2078	0.2219	-0.0141	0.00379671	t = -23.45, p = 6.69e-25
Unique alignment (%) *	83.2919	83.6016	-0.3017	0.03348539	t = -58.51, p = 6.50e-40

**Supplementary Table 5. Functional consequences predicted for 83,250 non-reference variants.** Variant consequences were predicted using VEP (version 91.3) based on a custom annotation file from Augustus. Only the most severe consequence is shown for each variant.

Variant consequence	SNPs	Indels	All	Proportion (%)
splice_acceptor_variant	4	1	5	0.006
splice_donor_variant	2	0	2	0.0024
frameshift_variant	0	26	26	0.0312
inframe_insertion	0	1	1	0.0012
inframe_deletion	0	4	4	0.0048
splice_donor_variant	2	0	2	0.0024
stop_gained	17	0	17	0.0204
stop_lost	1	0	1	0.0012
start_lost	3	0	3	0.0036
missense_variant	700	0	700	0.8408
splice_region_variant	45	1	46	0.0553
synonymous_variant	374	0	374	0.4492
stop_retained_variant	1	0	1	0.0012
coding_sequence_variant	2	0	2	0.0024
5_prime_UTR_variant	86	2	88	0.1057
3_prime_UTR_variant	1253	149	1402	1.6841
intron_variant	5809	443	6252	7.5099
upstream_gene_variant	2559	277	2836	3.4066
downstream_gene_variant	1811	179	1990	2.3904
intergenic_variant	61040	8458	69498	83.481
moderate impact	701	5	706	0.848
high impact	27	27	54	0.0649

## Supplementary Note 1

### Assembly of the Original Braunvieh (OBV) genome

The Original Braunvieh primary assembly was generated from PacBio HiFi CCS reads (study accession PRJEB42335 under sample accession SAMEA7759028), generated from subreads with minimum three passes and minimum predicted read quality of 20. The fastq data contained 86.9 gigabases, corresponding to nearly 30-fold coverage. The CCS reads were filtered by fastp [0.21.0] (3) with minimum average quality of Q20 and minimum read length of 1kb, with 99.99% of the data passing these thresholds. Hifiasm [v0.13-r308] (4) was then used to generate the assembly from the reads using the additional parameters “-r 4 -a 5 -n 5” on a computing cluster. Hifiasm yields the primary contigs in the GFA format, which were then converted using gfatools [0.4-r196-dirty] into a fasta sequence representation. These contigs were then scaffolded using RagTag [v1.0.1] (5) to the ARS-UCD1.2 reference, with custom parameters “--mm2-params "-c -x asm5" -r -m 1000000”.

The contigs were validated for contiguity, completeness, and correctness by multiple independent tools, available in a Snakemake [5.26.1] (6) pipeline online at <https://github.com/AnimalGenomicsETH/bovine-assembly>. Basic contiguity was determined through the *asmstat* command of pafutils (7). Similarly, the NGA50 value was determined through mapping the contigs to the ARS-UCD1.2 reference, and subsequently considering the length of alignment blocks again with *asmstat*. These values are described in Table SN1.

#### Table SN1: Contiguity metrics of the primary Original Braunvieh assembly.

Size refers to the total number of bases in the chromosomes and unplaced contigs. NG50 was calculated for both the contig set and the scaffolded assembly with the expected genome size taken from the ARS-UCD1.2 reference. Similarly, NGA50 is the NG50 value for aligned blocks of the assembly to the ARS-UCD1.2 reference.

	Size	Contig NG50	NGA50	Scaffold NG50	L50	Contigs
<b>assembly</b>	3.17gb	86.0	68.9	96.3	15	765

Completeness of the assembly was determined through two independent approaches, BUSCO (8) and the *asmgene* command of pafutils. The former relies on the OrthoDB datasets, specifically version 10 of the cetartiodactyla lineage. The latter uses cDNA libraries of annotated gene sequences from the ARS-UCD1.2 reference available from Ensembl. Both methods report a high completeness (>96%) with respect to predicted gene content, as shown in Table SN2.

**Table SN2: Predicted single-copy gene completeness of the primary Original Braunvieh assembly.**

Single-copy refers to genes that were correctly present once in assembly, while duplicates are genes which appeared more than expected. Fragmented genes are those which are only partially mapped, or fully mapped but split into multiple pieces. Missing genes are either not found or mapped below 10% of the expected gene.

	Single copy	duplicates	fragmented	missing	total
<b>Busco</b>	12533	283	166	353	13335
<b>asmgene</b>	18503	166	68	136	18873

Correctness was likewise determined by two k-mer based approaches, yak [r58] (4) and Merqury (9). Yak uses an approximate hash-table approach, while Merqury can be run in an exact mode. Both used short read sequences (2x150 bp) from the primary animal, which importantly were not used in generating the assembly, allowing for an independent evaluation. In addition, short read sequences from both parents enabled a quantification of the switch error rate. Only yak provided an estimate of the Hamming error rate, while only Merqury provides phased block statistics. An overview of these statistics is shown in Table SN3.

**Table SN3: K-mer based, reference-free validation of the primary Original Braunvieh assembly.**

Assembly quality value (QV) is given as a Phred quality score. Completeness estimates how many k-mers present in the short reads are found in the assembly contigs. The switch error rate is calculated differently by yak and Merqury, measuring the percent of wrongly phased adjacent SNPs in yak while in Merqury it measures the percent of wrongly phased haplotype-specific k-mers (“hap-mers”). There are more than 100 phase switches within a 20kb window (long-range switch). The Hamming error is the percent of SNP sites that are phased wrongly. The phase block statistic is the N50 after contigs have been broken at long-range switches, defined as more than 100 wrongly phased hap-mers per 20kb window.

	QV	Completeness	Switch error	Hamming error	Phased N50
<b>Yak</b>	48.76	100	0.012	0.37	-
<b>Merqury</b>	50.85	93.46	0.08	-	2.5 mb

Furthermore, the assembly was validated by comparing structural variants called by pbsv [2.4.0] between the reads and the ARS-UCD1.2 reference and those called by mumandco [v2.4.2] (10) between the assembly and the reference. There was good concordance between these approaches, for example an 8kb inversion identified in chromosome six of the assembly matched an 8kb inversion predicted by the read mapping.

The repeat content of the assembly was also in line with expectations, with approximately 48% of the assembly consisting of repeat elements or low complexity regions according to RepeatMasker version 4.1.1 (11) using the Repbase repeat database (release 20181026) (12). Several bovine-specific repeats were identified, along with telomeric or centromeric sequences not present in the existing ARS-UCD1.2 reference, indicating that several contigs are approaching chromosomal-scale and completeness.

## Supplementary Note 2

### Determination of the core and flexible parts of the pangenome graph

To investigate if the order of assemblies used to establish the multi-assembly graph impacts the core and flexible parts, we added the assemblies randomly to the graph. Core genome represents bases shared across all assemblies in the graph, while flexible genome represents number of bases that are variable across assemblies (i.e., not found in all assemblies) (13). The pangenome increased gradually with the number of assemblies added, driven by an increase in the flexible genome. The core genome size decreased from 2480 Mb to 2400 Mb in the full graph (Figure SN1), indicating that more genomic segments are variable across bovine species as we add more assemblies into the graph.

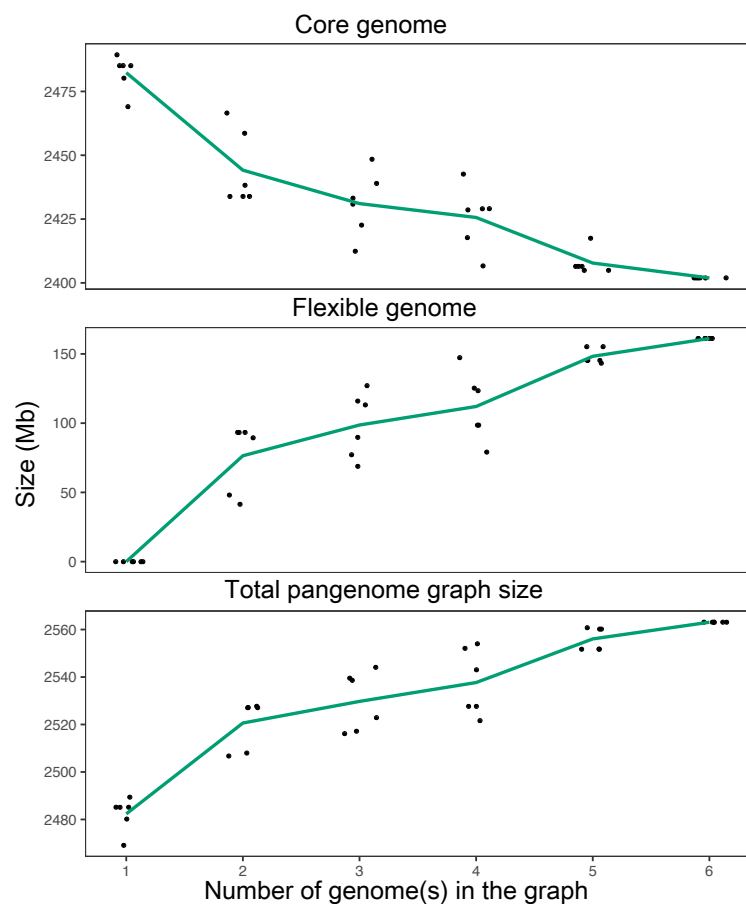


**Figure SN1. Profile of the multi-assembly graph with an increasing number of genomes integrated into the graph.** We varied the order and number of genomes added to the graphs, and calculated the number of bases in the pangenome, number of bases that are shared across all assemblies in the graph (core genome), and the number of bases that are variable across assemblies (i.e., not found in all assemblies, flexible genome). Points and lines indicate individual and average values.

Next, we investigated the profile of a multi-assembly graph that gradually increases in complexity. We built taurine-only graphs that contained either all or all but one taurine assemblies, a Taulnd (four taurine and one indicine), and a full graph (four taurine, one

indicine, and yak). The profile of the pangenome changed markedly as more distant assemblies were added to the graph. For example, the flexible part declined substantially from 6.10% in the full graph to 3.83% and 2.76% for the TauInd and taurine-only graph, respectively. However, when an individual taurine assembly is removed from the taurine-only graphs, the size of the flexible part changes only slightly (Figure SN2).

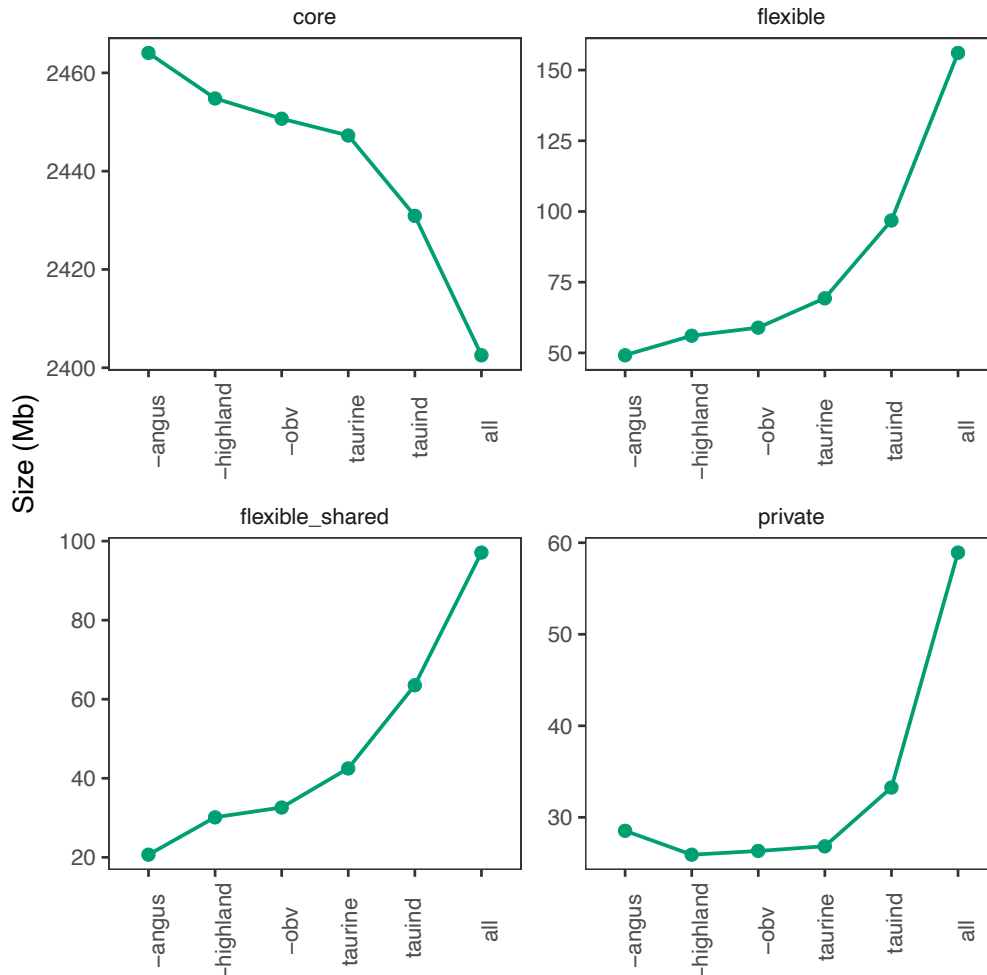


**Figure SN2. Pangenome profile as more distant assemblies are added to the graph.** The X-axis indicates the constructed graphs (- denotes the taurine assembly that was removed from the taurine-only graph, taurine denotes a graph with four taurine assemblies, the indicine graph contains all taurine assemblies and the assembly of Brahman, and all reflects a multi-assembly graph that contains all six assemblies (taurine, indicine, and yak). The core part is the size of the segments that are common to all assemblies, flexible\_shared indicates the size of segments shared by at least two but not all assemblies, and private denotes the size of segments found only in a single assembly, thus flexible genome is composed of flexible\_shared + private segment.



## Supplementary Note 3

### Construction of bovine multi-assembly graphs with different backbones

To investigate if the choice of the backbone assembly influences the properties of the bovine multi-assembly graph, we constructed six graphs, one for each possible assembly backbone. The remaining five assemblies were added according to their Mash-distance to the chosen backbone. Larger assembly backbones tended to result in larger multi-assembly graphs (see Table 1 in the main paper, Table SN4). The total number of non-reference bases detected varied between 63,745,420 bp and 72,349,303 bp for the OBV and Brahman backbone, with a mean value of 68.72 Mb and a standard deviation of 3.17 Mb. Fewer non-reference bases were detected when the OBV and Highland assemblies were used as backbones.

**Table SN4:** Properties of bovine multi-assembly graphs with different backbones

Parameter	Unit	Backbone Assembly					
		Hereford	Angus	Highland	OBV	Brahman	Yak
Nodes	n	182,940	182,332	183,118	184,098	184,301	188,975
Size	bp	2,558,596,439	2,540,507,180	2,550,176,720	2,671,491,862	2,549,613,449	2,547,048,782
Ref nodes	n	123,483	123,116	124,220	125,088	124,410	126,883
Ref length	bp	2,489,385,779	2,468,157,877	2,483,452,092	2,607,746,442	2,478,073,158	2,478,308,164
Nonref nodes	n	59,457	59,216	58,898	59,010	59,891	62,092
Non-ref length	bp	69,210,660	72,349,303	66,724,628	63,745,420	71,540,291	68,740,618
Edges	n	258396	257531	258608	260044	260209	266139
Edges/nodes	ratio	1.4125	1.4124	1.4122	1.4125	1.4119	1.4083
R-R edges	n	141,086	140,742	142,133	143,133	141,978	144,442
R-NR edges	n	113,332	112,669	113,116	114,058	114,064	114,837
NR-NR edges	n	3,978	4,120	3,359	2,853	4,167	6,860
core count	n	67,482	67,499	67,616	67,619	67,763	68,614
core length	bp	2,402,561,410	2,394,756,562	2,402,656,874	2,414,762,810	2,398,150,572	2,397,494,177
core prop	%	93.9	94.26	94.22	90.39	94.06	94.13
flexible count	n	115,458	114,833	115,502	116,479	116,538	120,361
flexible length	bp	156,035,029	145,750,618	147,519,846	256,729,052	151,462,877	149,554,605
flexible prop	%	6.10	5.74	5.78	9.61	5.94	5.87
CPU time	min	290.43	276.33	274.52	210.46	282.59	299.01
Max mem	Gb	55.03	58.88	55.6	58.31	56.67	56.96
Average mem	Gb	36.34	37.08	34.43	34.38	36.08	34.64
Run Time	min	41.78	39.4	41.23	30.6	39.35	42.7

The choice of the backbone had, as expected, a major impact on the amount of non-reference bases detected from each of the remaining assemblies (Table SN5). A multi-assembly graph with a *Bos taurus taurus* backbone contains between 10.14 and 19.48 million non-reference bases from the remaining three taurine assemblies. Using the Hereford

or Angus assemblies as the backbone resulted in more total non-reference sequences than using the OBV or Highland assemblies. Regardless of backbone choice, the OBV and Highland assemblies also contribute more non-reference sequences to the multi-assembly graph than the Hereford and Angus assembly. These two observations suggest that the OBV and Highland assemblies represent a more comprehensive *Bos taurus taurus* genome, agreeing well with their high completeness, continuity, and correctness (see Supplementary Note S1 and Rice *et. al.* (14)). Thus, there is a tendency to detect fewer non-reference sequences with a more complete and contiguous backbone. Although selecting a more distant assembly as the backbone identifies more non-reference sequences from each remaining assembly on average (~40 Mb with Yak compared to ~20 Mb for taurine), this appeared to be a smaller effect compared to the backbone completeness.

**Table SN5:** Non-reference bases detected (Mb)

Backbone	Assembly						
	Hereford	Yak	Brahman	OBV	Angus	Highland	Total <sup>1</sup>
Hereford	-	43.34	23.64	18.2	14.45	15.54	69.21
Yak	40.88	-	40.12	44	38.94	39.48	68.74
Brahman	23.09	42.11	-	24.62	21.23	21.7	71.54
OBV	11.91	39.64	17.69	-	10.14	11.18	63.75
Angus	17.99	44.02	23.40	19.48	-	16.94	72.35
Highland	13.03	40.09	20.27	14.21	11.64	-	66.72

<sup>1</sup>The total value is taken from the “Non-ref length” row of Table SN4.

Furthermore, the total length of each assembly’s private non-reference nodes, was barely affected by backbone choice. This suggests that our approach to building multi-assembly graphs with minigraph and labelling non-reference nodes work well regardless of choice of the initial backbone assembly (Table SN6).

**Table SN6:** Total length in Mb of private non-reference nodes.

Backbone	Assembly					
	Hereford	Yak	Brahman	OBV	Angus	Highland
Hereford	-	29.9	8.22	4.61	2.39	2.78
Yak	4.36	-	8.62	5.05	2.47	2.93
Brahman	4.69	30.26	-	4.85	2.69	3.19
OBV	4.33	30.02	8.34	-	2.67	3.02
Angus	4.60	29.85	8.20	5.01	-	2.76
Highland	4.40	29.85	8.14	4.75	2.38	-

## Assessment of the sequences not included in the graphs

Minigraph might fail to align and include input sequences into the graph. We assessed bases not included in the graph by comparing the total realignment size of the assembly to the graphs with the total pangenome size. All bases in the backbone are included in the multi-assembly graph, but this is not the case for the additional assemblies which subsequently augment the graph (Table SN7). We again found that the use of the Original Braunvieh backbone led to fewer non-reference bases not included in the graph from each remaining assembly.

**Table SN7:** Total assembly sequences (bp) not included in the graphs.

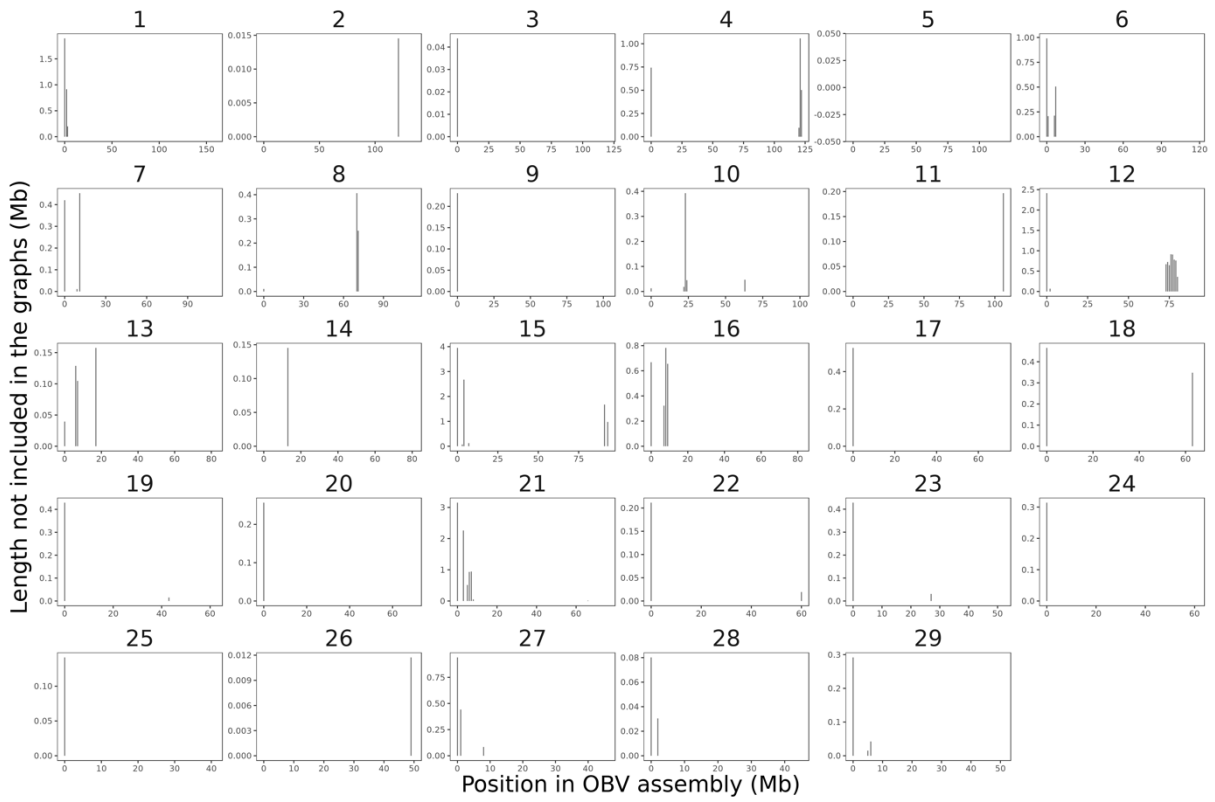
Backbone	Assembly						Total
	Hereford	Yak	Brahman	OBV	Angus	Highland	
Hereford	-	5,388,777	6,369,649	106,905,680	7,442,463	8,165,867	134,272,436
Yak	15,420,157	-	9,466,221	116,311,772	8,286,464	10,732,937	160,217,551
Brahman	17,427,243	9,103,978	-	111,856,939	12,067,771	12,108,523	162,564,454
OBV	9,716,932	2,690,446	3,339,031	-	882,571	4,659,329	21,288,309
Angus	26,973,081	18,470,665	20,032,971	115,587,224	-	20,796,186	201,860,127
Highland	13,401,923	6,069,608	7,053,961	104,868,806	6,680,628	-	138,074,926

The Original Braunvieh assembly has between 105 and 116 Mb of sequences which are not augmented into the different multi-assembly graphs. We investigated which parts of the OBV assembly were not included in the Hereford-backbone graph using the reverse mapping approach enumerated below:

1. Extract nodes in the graph covered with OBV alignment
2. Map the sequence in the node to the OBV assembly using minimap2
3. Collect region longer than 10kb with no coverage from the alignment
4. Visualize the region across OBV genome region

As shown in figure SN3, many sequences not included in the graph are located at the start or end of chromosomes, which might indicate that the HiFi reads enabled a better (more complete) assembly of telomeric or centromeric regions. This hypothesis is further supported by a repeatmasker analysis revealing that these regions contain many DNA satellite (21,139,818 bp) and retroelements (7,774,559 bp).

**Figure SN3.** The location of sequences from the Original Braunvieh assembly not included in the graph. Numbers above the plot denote chromosomal identifiers.



## Supplementary Note 4

### Differential expression analysis

We tested 13,085 genes that were expressed  $\geq 1$  CPM in at least eight samples (sample size from each group) for differential expression between *Mycobacterium bovis*-infected and non-infected control animals. We detected (adjusted FDR  $\leq 0.05$ ) 1,769 and 1,877 genes that were up- and down-regulated respectively in peripheral blood leukocytes of *Mycobacterium bovis*-infected cattle (Figure SN4). Of 12,813 genes of the Ensembl ARS-UCD1.2 genome annotation that were expressed at  $\geq 1$  CPM in at least eight samples, 3610 (28.17%) were differentially expressed. Of 272 putatively novel genes that were expressed  $\geq 1$  CPM in at least 8 samples, 36 (13.23%) were differentially expressed.

We found that genes relevant for the immune response were among the top differentially expressed genes with the greatest mean log-fold change (e.g., DEFB10 -8.24-fold, CXCL10 -3.30-fold, IL12B -3.11-fold, CXCL5 7.11-fold, CTLA4 4.25-fold, and CXCL8 5.70-fold), matching observations on an older reference genome annotation by McLoughlin *et al.* (15) Table SN8. Multidimensional scaling (MDS) representations of transcript abundance estimates from either all 13,085 genes (Figure SN5b) or 3646 differentially expressed genes (Figure SN5a) separated *Mycobacterium bovis*-infected from healthy cattle. We discovered more differentially expressed genes of the Ensembl ARS-UCD1.2 genome annotation than McLoughlin *et al.* (15) (3610 vs. 3250), likely due to a vastly improved genome assembly (27,115 vs. 24,616 genes are included in build 101 (ARS-UCD1.2) and build 73 (UMD3.1), respectively). Using data from the supplement provided by McLoughlin *et al.*, we were able to compare the expression levels of 2678 (out of 3250) differentially expressed genes between different genome builds (UMD31, standard and extended ARS-UCD1.2) and annotations (Figure SN6). Six genes with the greatest fold-change increase in expression reported by McLoughlin *et al.* had a very similar expression pattern from all assemblies considered.

**Table SN8:** The expression of 6 immune genes reported by McLoughlin *et al.* across different assemblies.

Ensembl gene ID	Gene symbol	Log <sub>2</sub> FC UMD3.1 (McLoughlin <i>et al.</i> )	Log <sub>2</sub> FC Standard ARS-UCD1.2	Log <sub>2</sub> FC Extended ARS-UCD1.2
ENSBTAG00000019716	CXCL8	2.435	2.512	2.512
ENSBTAG00000009812	CXCL5	2.763	2.831	2.831
ENSBTAG00000013170	CTLA4	1.849	2.088	2.088
ENSBTAG00000004741	IL12B	-2.129	-1.841	-1.841
ENSBTAG00000048737	DEFB10	-2.850	-3.042	-3.042
ENSBTAG00000001725	CXCL10	-1.712	-1.722	-1.722

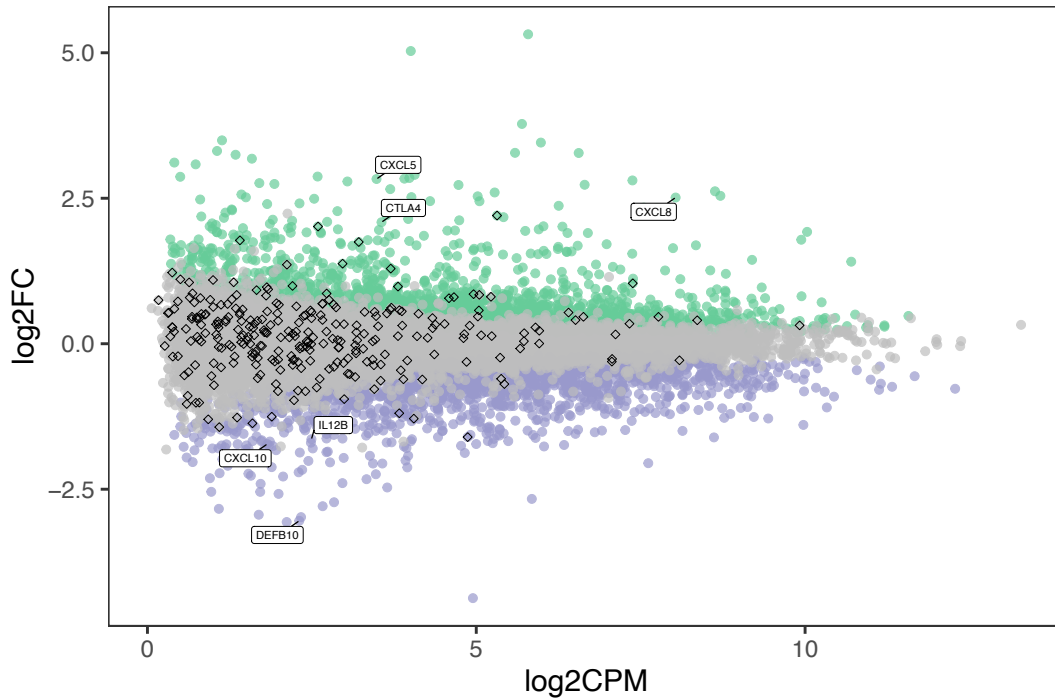


**Figure SN4. Smear plot from the differential expression analysis.** Grey, green, and purple color indicates genes with no expression difference, significant up-regulation, and down-regulation in peripheral blood leukocytes of *Mycobacterium bovis*-infected cattle. Diamonds indicate 272 putatively novel genes assembled from RNA sequencing reads mapping to non-reference sequences. Six genes reported by (McLoughlin *et al.* 2014) are indicated with the text labels.

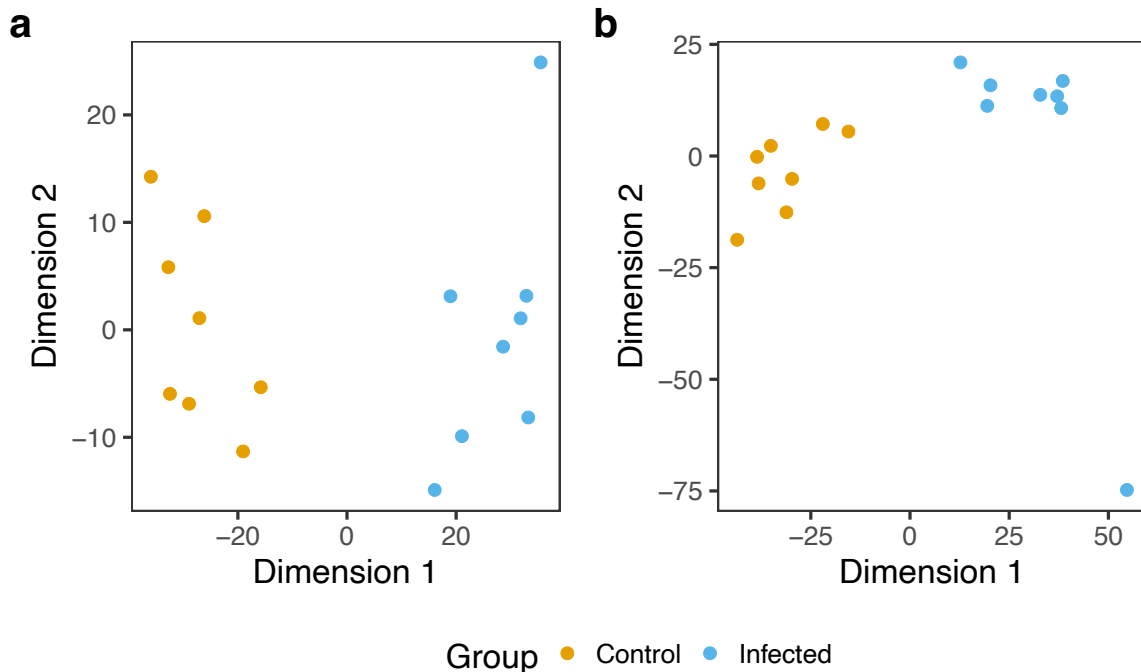


**Figure SN5. Multidimensional scaling analysis (MDS) based on transcript abundance estimates of (a) 3646 differentially expressed, and (b) 13,085 genes with CPM $\geq$ 1 in eight samples.** Each point represents an individual *Mycobacterium bovis*-infected (blue) or control (orange) sample.

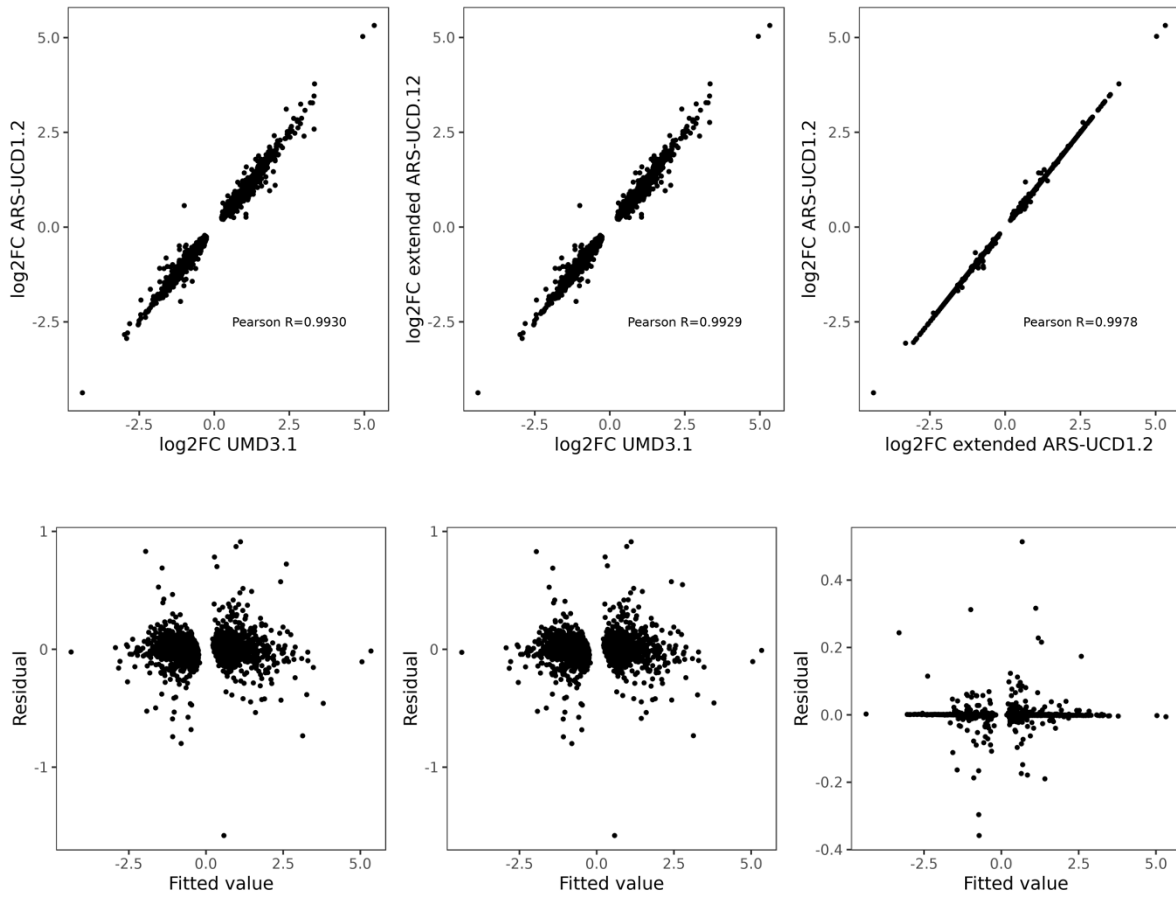


**Figure SN6. Log<sub>2</sub>FC expression of 2678 genes between UMD3.1 (as reported in McLoughlin *et. al*), the standard ARS-UCD1.2, and extended ARS-UCD1.2 reference. Each point indicates the expression of a gene.**

## Supplementary Note 5

### Detailed description of the analysis workflow presented in the main paper

Step by step (manual) instruction to construct a multi-assembly graph from a collection of genome assemblies and characterize its structural variations. All steps can be automatically invoked with a workflow from a Github repository (<https://github.com/AnimalGenomicsETH/bovine-graphs>).

#### *Pangenome graph construction*

1. Estimate pairwise genetic distance between the assemblies

```
# sketch assembly, done separately for each assembly
mash sketch -p {threads} -o {output} {input_assembly}

# combined all sketches
mash paste {output} {input_sketch1} {input_sketch2}

# estimate distance based on combined sketches
mash dist {input_combined_sketch} {input_combined_sketch} > {output_distance}

# visualize the genetic relationship as a tree (optional)
scripts/phylo_tree_assembly.R
```

2. Graph construction

Assemblies are added to the graph based on their genetic distance to the backbone assembly. Less distant assemblies are added before the more distant ones.

```
# graph construction
minigraph --inv no -xggs -t {threads} {input_assembl} {input_assemb2} > {graph.gfa}

# subset graph file for easier access of nodes and edges information
# without the need for loading the sequences in nodes

# extract node information
awk '$1~/S/ { split($5,chr,":"); split($6,pos,":"); split($7,arr,":");
print $2,length($3),chr[3],pos[3],arr[3] }' {graph.gfa} > {graph_len.tsv}

# extract edge information
awk '$1 == "L"' {graph.gfa} > {graph_link.tsv}
```

3. Re-align each assembly to the multi-assembly graph

Separately realign each assembly to the multi-assembly graph to record the coverage for all nodes and edges in the graph.



```
minigraph -t {threads} --cov -x asm {graph.gfa} {assemb1.fa} > {graph_use_assemb1.gfa}
```

```
minigraph -t {threads} --cov -x asm {graph.gfa} {assemb2.fa} > {graph_use_assemb2.gfa}
```

#### 4. Combine node and edge coverage across assemblies

```
# custom python script  
scripts/comb_coverage.py -g {assemb1} {assemb2} -a {graph_name}  
#output node_coverage.tsv and edge_coverage_use.tsv
```

#### 5. Use coverage data to label the nodes in the graph

```
# custom R script  
scripts/colour_node.R {assemb1} {assemb2} {graph_name}
```

Output:

- *nodecol.tsv* containing node and label information

Node	Labels
S1	Assemb1
S2	Assemb1, Assemb2

- *nodemat.tsv* containing presence (1) and absence (0) of the label in each node

Node	Assemb1	Assemb2
S1	1	0
S2	1	1

#### 6. Analyze the properties of the multi-assembly graph based on the node and edge labels

```
# custom R script  
scripts/run_core_nonref.R {graph_name}
```

Four R functions will be invoked, which are detailed as below:

Function	Description	Output file
calculate core	calculate the proportion of core and flexible parts of pangenome	core_analysis.tsv
pangenome sampling	evaluate the graph properties as more assemblies being added to the graph	core_flex_sim.tsv
calculate non_ref	calculate the non-ref node length from each assembly	nonref_analysis.tsv

nonref_sharing_pattern	make plots of the non-ref node sharing across assemblies	nonref_shared_len.pdf
------------------------	--	-----------------------

## Structural variant analysis

### 1. Identify bubbles in the graph

Bubbles are regions that diverged between assemblies which have a common start and stop node derived from reference sequences.

```
gfatools bubble {graph.gfa} > {bubble.tsv}
```

### 2. Identify the precise location of the structural variations from the multi-assembly graph

Paths in the bubble represent alleles of the structural variations. This step will enumerate all possible paths based on the start and stop node of the bubbles, done separately for biallelic (2 paths/alleles) and multi-allelic ( $\geq 3$  alleles) bubbles. Finally, it labels structural variations according to the origin of the assemblies.

```
# custom Python scripts
# biallelic SV
scripts/get_bialsv.py -a {assemb1} {assemb2} > {output}
#output: biallelic_sv.tsv

# multiallelic SV
scripts/get_multisv.py -a {assemb1} {assemb2} > {output}
#output: multiallelic_sv.tsv

#trace path in each SV according to the origin of the assemblies
scripts/trace_path.py -g {assemb1} {assemb2} -a {graph_name} > {output}
```

### 3. Annotate the breakpoints detected in from the multi-assembly graph

Annotate the breakpoint of the structural variations using start and stop node coordinate for left and right breakpoints, respectively on the reference backbone coordinate. This step requires an annotation file from the backbone assembly.

```
# custom Python script
scripts/annot_breakpoints.py #output bubble_annot.tsv
```

#### 4. Extract structural variation alleles in the bubbles

Extract non-ref alleles (excluding paths less than 100 bp, complete deletions, or paths without non-ref sequences) as a representative non-reference sequences of the pangenome. Sequences in nodes are not used directly, because multiple consecutive nodes might be part of the same allele, and they are representing a continuous sequences.

```
#custom Python scripts

# biallelic allele extraction
scripts/get_bialseq.py -a {assembl1} {assemb2} #output bialsv_seq.fa

# multiallelic allele extraction
scripts/get_multiseq.py -a {assembl1} {assemb2} # output multiseq.fa

# combined biallelic and multiallelic SV sequences as the representative of the non-ref sequences
cat {bialsv_seq.fa} {multiseq.fa} > {nonref_seq.fa}
```

## SI References

1. A. Heger, K. Jacobs, Pysam Documentation. 1–39 (2018).
2. D. Crysanto, H. Pausch, Bovine breed-specific augmented reference graphs facilitate accurate sequence read mapping and unbiased variant discovery. *Genome Biol.* **21** (2020).
3. S. Chen, Y. Zhou, Y. Chen, J. Gu, fastp : an ultra-fast all-in-one FASTQ preprocessor. *Bioinformatics*, 274100 (2018).
4. H. Cheng, G. T. Concepcion, X. Feng, S. Garg, Haplotype-resolved de novo assembly with phased assembly graphs. *arXiv*, 1–10 (2020).
5. M. Alonge, *et al.*, RaGOO: Fast and accurate reference-guided scaffolding of draft genomes. *Genome Biol.* **20** (2019).
6. J. Köster, S. Rahmann, Snakemake--a scalable bioinformatics workflow engine. *Bioinformatics* **28**, 2520–2522 (2012).
7. H. Li, Minimap2: Pairwise alignment for nucleotide sequences. *Bioinformatics* **34**, 3094–3100 (2018).
8. M. Seppey, M. Manni, E. M. Zdobnov, “BUSCO: Assessing genome assembly and annotation completeness” in *Methods in Molecular Biology*, (2019) [https://doi.org/10.1007/978-1-4939-9173-0\\_14](https://doi.org/10.1007/978-1-4939-9173-0_14).
9. A. Rhie, B. P. Walenz, S. Koren, A. M. Phillippy, Merqury: Reference-free quality, completeness, and phasing assessment for genome assemblies. *Genome Biol.* **21**, 1–27 (2020).
10. S. O’Donnell, G. Fischer, MUM&Co: Accurate detection of all SV types through whole-genome alignment. *Bioinformatics* (2020) <https://doi.org/10.1093/bioinformatics/btaa115>.
11. A. Smit, R. Hubley, P. Green, RepeatMasker Open-4.0 (2015) (January 8, 2021).
12. W. Bao, K. K. Kojima, O. Kohany, Repbase Update, a database of repetitive elements in eukaryotic genomes. *Mob. DNA* **6** (2015).
13. A. A. Golicz, P. E. Bayer, P. L. Bhalla, J. Batley, D. Edwards, Pangenomics Comes of Age: From Bacteria to Plant and Animal Applications. *Trends Genet.* **36**, 132–145 (2020).
14. E. S. Rice, *et al.*, Continuous chromosome-scale haplotypes assembled from a single interspecies F1 hybrid of yak and cattle. *Gigascience* **9** (2020).
15. K. E. McLoughlin, *et al.*, RNA-seq transcriptional profiling of peripheral blood leukocytes from cattle infected with *Mycobacterium bovis*. *Front. Immunol.* **5** (2014).